Available online at www.sciencedirect.com

ScienceDirect

journal homepage: www.elsevier.com/locate/he

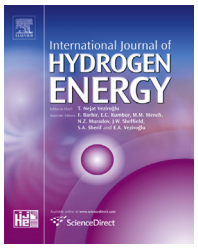

Additive manufacturing of liquid/gas diffusion layers for low-cost and high-efficiency hydrogen production☆

Jingke Mo [a], *Ryan R. Dehoff* [b], *William H. Peter* [b], *Todd J. Toops* [b], *Johney B. Green Jr.* [b], *Feng-Yuan Zhang* [a,*]

[a] *Nanodynamics and High-Efficiency Lab for Propulsion and Power, Department of Mechanical, Aerospace & Biomedical Engineering, UT Space Institute, University of Tennessee, Knoxville, Tullahoma, TN 37388, USA*
[b] *Oak Ridge National Laboratory, 1 Bethel Valley Rd., Oak Ridge, TN 37831, USA*

ARTICLE INFO

Article history:
Received 9 November 2015
Accepted 6 December 2015
Available online 14 January 2016

Keywords:
3D printing
Electron beam melting additive manufacturing
Proton exchange membrane electrolyzer cell
Liquid/gas diffusion layers
Multifunctional materials

ABSTRACT

A low-cost additive manufacturing technology, electron beam melting (EBM), is employed for the first time to fabricate titanium liquid/gas diffusion media with high-corrosion resistances and well-controlled multifunctional parameters, including two-phase transport and high electric/thermal conductivities. Its application in proton exchange membrane electrolyzer cells (PEMECs) has been investigated *in-situ* with modular galvano (MG) and galvano electrochemical impedance spectroscopy (GEIS) and characterized *ex-situ* with SEM and XRD. Compared with conventional woven and sintered liquid/gas diffusion layers (LGDLs), much better performance is obtained with EBM-fabricated LGDLs due to a significant reduction of ohmic losses. The EBM technology components exhibited several distinct advantages in fabricating LGDLs: well-controllable pore morphology and structure, rapid prototyping, fast manufacturing, highly customizable design, and economic. In addition, by taking advantage of additive manufacturing, it is possible to fabricate complicated three-dimensional designs of virtually any shape from a digital model into one single solid object faster, cheaper, and easier, especially for titanium components. More importantly, this development will provide LGDLs with well-controllable pore morphologies, which will be valuable to develop sophisticated models of PEMECs with optimal and repeatable performance. Furthermore, it could lead to a manufacturing solution that greatly simplifies the PEMEC/fuel cell components.

☆ This manuscript has been authored in part by UT-Battelle, LLC, under Contract No. DE-AC05-00OR22725 with the U.S. Department of Energy. The United States Government retains and the publisher, by accepting the article for publication, acknowledges that the United States Government retains a non-exclusive, paid-up, irrevocable, world-wide license to publish or reproduce the published form of this manuscript, or allow others to do so, for United States Government purposes.

* *Corresponding author*. Tel.: +1 931 393 7428.
E-mail address: fzhang@utk.edu (F.-Y. Zhang).

http://dx.doi.org/10.1016/j.ijhydene.2015.12.111

Introduction

With a high energy density and no harmful emissions, hydrogen has the potential to play an important role as an energy carrier in the future [1–7]. However, hydrogen is not an energy source; it doesn't exist in nature in its elemental or molecular form; therefore, hydrogen must be produced. Proton exchange membrane (PEM) water electrolysis, which was first developed in the mid-1970s by General Electric based on the first solid polymer electrolyte system deployed the Gemini Space Program [8], has been among the most efficient and practical means of producing hydrogen to date. In recent years this technology has been developed significantly and has become more attractive to produce hydrogen from water and to store energy by taking advantage of renewable energy sources and new material innovations. Proton exchange membrane electrolyzer cells (PEMECs) have a number of advantages compared to other electrolysis processes, including production of hydrogen at a higher purity, capable of operation at higher current density on the electrodes leading to faster reaction, and the ability to operate at pressures up to 200 bar thus providing the advantage of delivering the hydrogen at a high pressure for the end user. These benefits all contribute to the choice of PEM based electrolysis as the best method to supply hydrogen [9–12].

A PEMEC consists of a catalyst-coated membrane sandwiched between anode and cathode electrodes. Each electrode includes a catalyst layer (CL), a liquid/gas diffusion layer (LGDL), and a bipolar plate (BP), which also acts as the current distributor (CD) and the flow field. When a sufficient electrical current is applied, water decomposes to oxygen, protons, and electrons at the anode reaction site. Protons pass through the membrane, typically Nafion, to the cathode and react with electrons to form hydrogen. By combining single cells, a PEMEC stack can supply huge amounts of hydrogen and oxygen that can be stored for later use.

One of key challenges for current PEMECs is to improve the performance and cost efficiency with the most suitable LGDLs, which are located between the catalyst layers (CLs) and the bipolar plate (BP)/current distributor (CD) in a PEMEC, as shown in Fig. 1. The LGDLs are expected to transport reactants, electrons, heat, and products, with minimum voltage, current, thermal, interfacial, and fluidic losses [13–20]. The LGDL has to meet the following challenges: (1) Reactant permeability: provide reactant water access effectively from flow channels to catalyst layers; (2) Product permeability: provide flow pathways for H_2/O_2 from catalyst-layer area to flow channels; (3) Electronic conductivity: provide electrons to all reaction sites; (4) Thermal conductivity: provide efficient heat transport and uniform heat distribution; and (5) Interfacial and mechanical properties: provide high corrosion resistance and good contacts (i.e., good interfacial electrical and thermal conductivity) with the adjacent materials/parts (BP/CD and CL), and maintain small pressure drops in the flow channel. Thus, effective LGDLs will promote a uniform current/thermal distribution at the adjacent reaction sites.

Carbon materials (carbon paper or carbon cloth), which are typically used in PEM fuel cells (PEMFCs), are unsuitable for PEMECs due to the high potential of the oxygen electrode [21]. Metallic LGDLS and bipolar plates have attracted more interest in both PEMECs and PEMFCs due to their high conductivity, rapid production, and low cost [22–24]. By taking advantage of novel designs and advanced fabrication methods, a thin-film metallic LGDL with well-controlled pore morphologies and surface properties demonstrated good functionality and water management in PEMFCs [22,25–27]. However, since material corrosion and consumption will result in poor interfacial contacts, degrading the PEMEC performance and efficiency, metallic LGDLs with higher corrosion resistance are strongly desired.

Titanium has received considerable attention as a promising structural/functional material in aerospace, marine, nuclear, electronics, medical implants, and instruments due to its high corrosion resistance even at high positive overpotentials as well as in highly acidic and humid conditions; however, difficulty in the machining of titanium and its cost have been limiting factors for its widespread application. With the development of additive manufacturing (AM) technology, which has the advantages of high precision, complex geometry capability, good repeatability, tooling-free, low-cost, and rapid batch production, several fabrication solutions for multifunctional and well-tunable LGDLs have become possible [28–30]. The electron beam melting (EBM) technology, which was commercialized by Arcam AB Corporation about 15 years ago, has greatly enhanced the AM capabilities by taking advantage of precisely-controlled and high-energy electron heating sources.

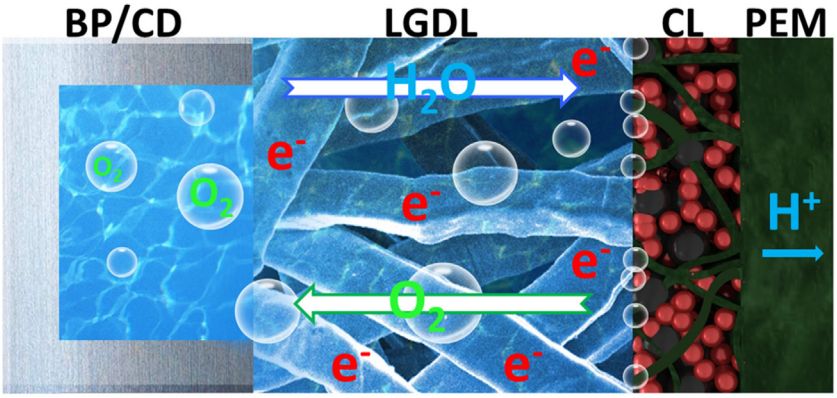

Fig. 1 – Schematic of LGDL functions at anode side.

The EBM process can be utilized to fabricate complex microstructures not possible through conventional AM methods. Its well-controllable process parameter window coupled with layer-by-layer fine powders offers a significant flexibility in designing parameters for various materials with complex internal microstructures and network. The EBM process has been explored previously for use in medical applications where non-stochastic mesh structures have been explored to mimic the mechanical response of bone. In addition, the mesh structure can also be altered to maximize the amount of bone adhesion when implanted in the body. To authors' knowledge, the EBM additive manufacturing of titanium-based components of PEMFCs/PEMECs has seldom been publicly reported. In this study, a titanium porous medium with controllable thickness and pore morphology was first developed with the EBM additive manufacturing for its application in PEMECs.

Experimental details

A PEMEC was designed and fabricated in lab to conduct the experiments. It mainly consists of two endplates made from commercial grade aluminum and designed to provide even compression pressure on the cell. In order to apply a current to the cell, a copper plate was inserted at the cathode as a current distributor. The cathode bipolar plate was fabricated from graphite and used a parallel flow field. The anode bipolar plate was fabricated from grade 2 titanium, and used a parallel flow field to distribute the flow over the active area of the cell. The titanium plate also has a function as the current distributor, as shown in Fig. 2. In an attempt to maintain even compression and prevent leakage, gaskets for the LGDLs were fabricated from polyvinyl chloride (PVC). The cell was compressed by eight evenly distributed bolts, which were tightened to 4.52 N m of torque during assembly. It has been verified by testing that the interfacial contact is good enough under this torque, further increasing the assemble torque won't reduce the total ohmic resistance. The electrolyzer had an active area of 5 cm^2 and was operated at room temperature.

Testing apparatus

The PEMEC was attached to an electrolyzer control system with a current range up to 100 A and a voltage range up to 5 V. The hardware was connected to EC-Lab, an electrochemical analysis software from Bio-Logic, which was used to evaluate performance and electrochemical impedance spectroscopy (EIS). For controlling the flow, a system of piping was connected to the PEMEC. While the cathode piping was merely intended to safely exhaust hydrogen gas that formed during electrolysis, a diaphragm liquid pump from KNF Neuberger was used to supply deionized water at a constant volumetric flow rate of 40 ml/min to the anode.

X-ray diffraction

The characterization of material structure and phase identification was carried out via x-ray diffraction (XRD) with a Philips X'Pert materials research diffractometer (45 kV, 40 mA), controlled by PANalytical's XRD software, in Bragg Brentano reflection geometry with Cu $K\alpha$ radiation ($\lambda = 1.5418$ Å) and a 2θ scan from 30° to 80° (with 0.01° steps for 5 s). The diffraction patterns are analyzed by the software MDI Jade9.

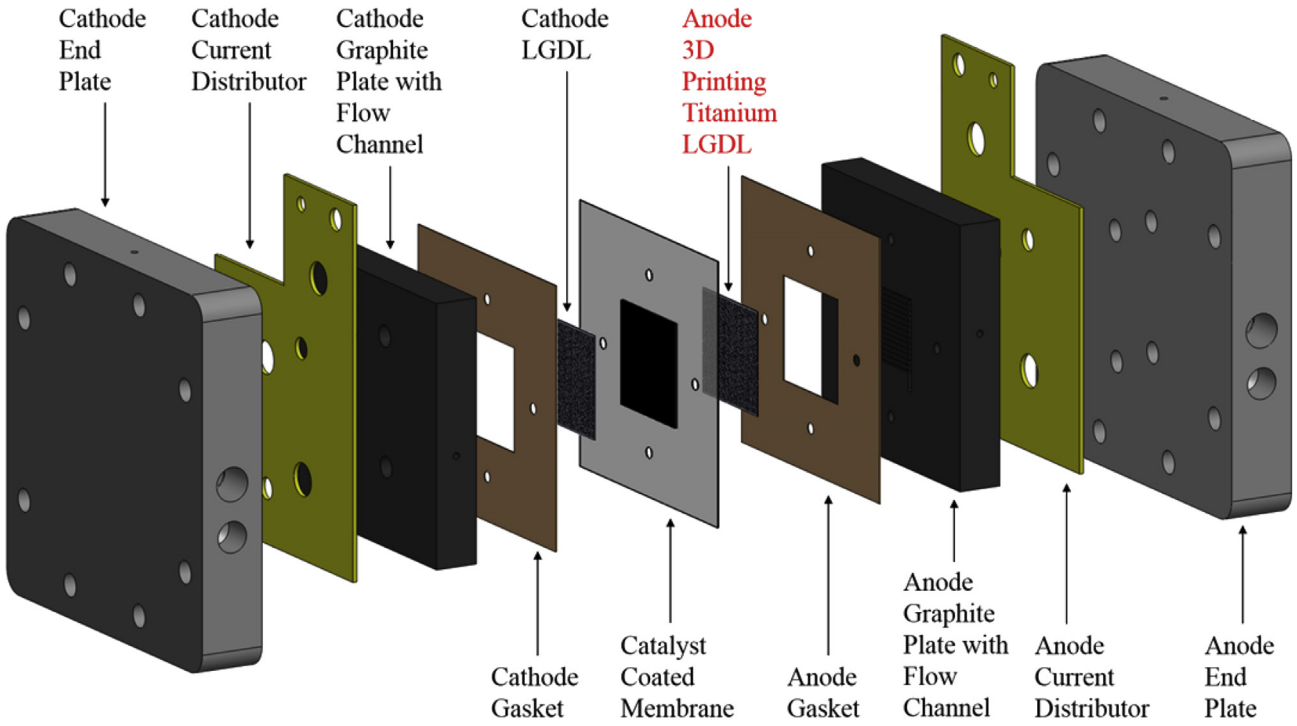

Fig. 2 – Schematic of PEMEC with LGDL of EBM Ti-6Al-4V mesh.

Scanning electron microscopy

The morphological characteristics of the gas diffusion layers and catalyst-coated membranes used in evaluation were observed using a field emission SEM. The SEM used was a JEOL JSM-6320F with an accelerating voltage of 0.5–30 kV, a magnification range of 500x up to 650,000x, and a 5-axis specimen mount. The working distance ranged from 25 mm to 6 mm. Images were captured, processed, and analyzed by TEAM software.

Performance testing

For performance evaluation, an increasing current density was applied to the PEMEC over a period of time. The current was stepped up from a current density of 0.2 A/cm^2 to 2.0 A/cm^2. At each current density, the potential of the cell was measured for five minutes before incrementing the current density again. Five minutes was chosen as an acceptable amount of time at each current density as it was empirically observed that the cell potential remained stable after this length of time.

Electrochemical impedance spectroscopy

Galvanostatic electrochemical impedance spectroscopy (GEIS) was used for measuring the impedance of the PEMEC at different operating conditions. In this method, the current is controlled as opposed to the potential. The test station is equipped with an operating current range of −100 A to +100 A and a voltage range of 0 V to 5 V. The current precision was 100 fA. The scanning frequency was varied from 10 kHz to 5 mHz, and recorded six points of data per decade. For analyzing impedance data, a Nyquist plot is normally used. There are normally two characteristic arcs in a typical Nyquist plot of the impedance of a PEMEC, which split the graph into three distinct ranges of high, medium, and low frequency. The leftmost x-intercept represents the ohmic losses of the PEMEC, and is generally measured for frequencies of a few kHz. The medium frequency range encompasses activation and charge-transfer losses in the electrolyzer, and has a characteristic frequency located in the local minima between the two arcs, and can range from 1 to a few hundred Hz. The low frequency region represents the mass-transfer losses in the PEMEC, and is at frequencies below 1 Hz.

3D printer

The electron beam melting technology, developed by Arcam AB, is a powder bed additive manufacturing technology in which titanium powder materials are spread into a 50-μm thick layer and subsequently melted by a focused electron beam. The geometry of the melted region is determined by the 2-dimensional cross section of a 3-dimensional component. Successive layers are built on top of a stainless steel substrate in order to fabricate a 3-dimensional component. The powder used in the process, Ti-6Al-4V, is a heavily used aerospace and biomedical alloy. The powder particle size distribution was 45 μm–105 μm and was plasma atomized powder supplied by Arcam AB. The samples were fabricated on an Arcam electron beam melting Q10 machine using software version 4.1.47. Because the melted area of the cross section is below a certain size threshold the entire structure is melted only with the contour melt theme and no bulk filling of the structure occurs. This results in the entire structure being melted as a series of spots along the contour of the stereo lithography (.stl) file. The outer contour is melted at 4.5 mA and the inner contour is melted using 8 mA. The standard focus values for this software version were used, and the resulting spot size of the electron beam is estimated to be on the order of 100–150 μm. Using these processing parameters resulted in a minimum wall thickness on the order of 100 s μm.

Finer structures may be obtainable through optimizing the processing parameters; however, preliminary work on this has indicated this may lead to porosity in the wall. The size and shape of the unit cell determines the final geometry of the component fabricated. The process has been explored previously for use in medical applications where non-stochastic mesh structures have been explored to mimic the mechanical response of bone, and the mesh structure can also be altered to maximize the amount of bone adhesion when implanted in the body. For this particular study, a non-stochastic grid of various sizes was utilized with identical cross section in the vertical build direction.

Results and discussion

Before *in-situ* testing, the titanium LGDL samples from the 3D printer were characterized with SEM and XRD. Fig. 3 shows typical images of an additively manufactured titanium LGDL, which has a thickness of 300 μm, a square pore size of 1.5 mm, and a pore-wall width of 500 μm. It should be noted here that the pore-wall width, pore size and pore distribution can be easily changed by altering the design parameters of the models, and/or varying fabrication conditions and powder sizes, thus obtaining expected porosities. In the high-resolution images shown in Fig. 3(B) and (C), the titanium powder can be clearly observed at the side walls of the pores. The top and bottom surfaces are smooth and flat with uniform thickness, which markedly improves the contact interface thereby reducing the contact resistance between the LGDL and catalyst layer. These features significantly distinguish the 3D printed LGDL from woven or welded LGDLs, as shown in Fig. 4. The wires crimp on both sides and are locked together at the wire joints for stability.

The XRD patterns of the EBM Ti-6Al-4V LGDL are shown in Fig. 5, which show titanium crystalline nature with 2θ peaks lying at 35.09° (100), 38.42° (002), 40.17° (101), 53.00° (102), 62.95° (110), 70.66° (103), 76.22° (112), and 77.37° (201). All the peaks in the XRD patterns can be indexed as hexagonal alpha phases of titanium and the diffraction data is in strong agreement with Joint Committee on Powder Diffraction Standards (JCPDS) files # 44-1294 and reference. [31] Crystallite size can also be obtained based on the Scherrer equation:

$$\tau = \frac{K\lambda}{\beta \cos\theta} \quad (1)$$

where τ is the crystal size; λ is the wavelength of the X-ray radiation ($\lambda = 0.15406$ nm) for Cu Kα; K is usually taken as 0.9;

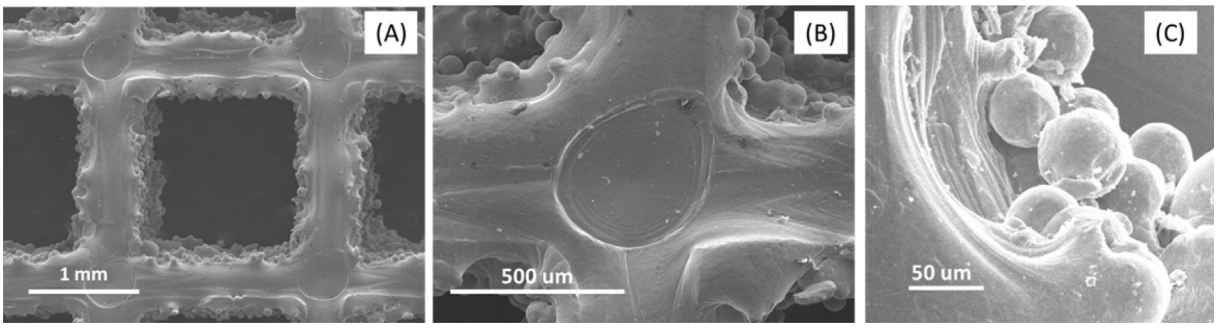

Fig. 3 – Images of EBM Ti-6Al-4V mesh LGDL at different scales.

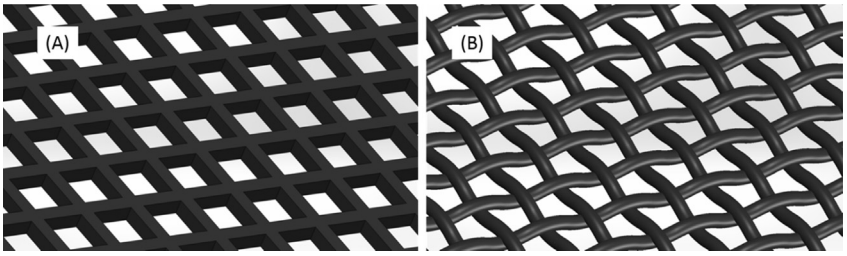

Fig. 4 – Schematic of LGDLs, (A) EBM Ti-6Al-4V mesh, (B) woven mesh.

and β is the line width at half-maximum height. The crystallite sizes obtained using this formula are from 18 to 32 nm.

In the PEMEC tests, EBM Ti-6Al-4V LGDLs were used at the anode and Toray 090 carbon paper treated with 5% PTFE was used as the cathode LGDL. For comparison, titanium woven mesh, which has similar wire thickness and porosity, was chosen to serve as a reference LGDL. Similar to EBM Ti-6Al-4V structures, woven meshes were used as the anode gas diffusion layer, and were tested in the same PEMEC and operating conditions. The effect of the LGDL with different fabrication process and structure at the anode on the PEMEC performance at room temperature is shown in Fig. 6. The operation voltages for both LGDLs were increased linearly with current densities from 0.2 A/cm^2 to 2.0 A/cm^2, where ohmic losses limit performance. Better performance (lower voltage) was obtained with EBM Ti-6Al-4V LGDL. At 1.5 A/cm^2, the operating voltage decreased from 2.49 V to 2.18 V, corresponding to more than 12% of an efficiency improvement.

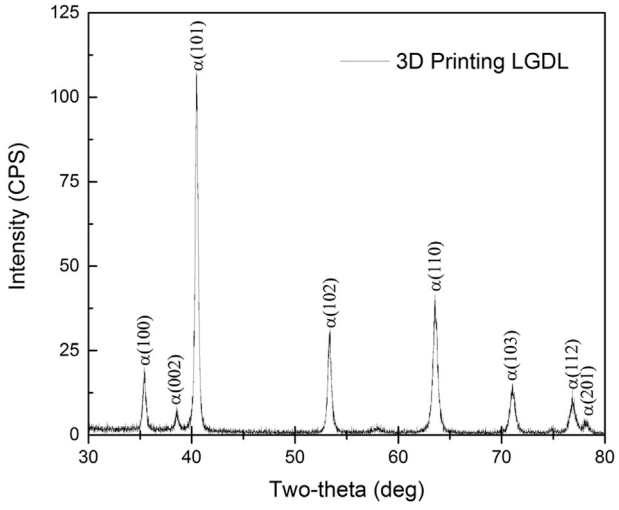

Fig. 5 – XRD Pattern of EBM Ti-6Al-4V mesh LGDL.

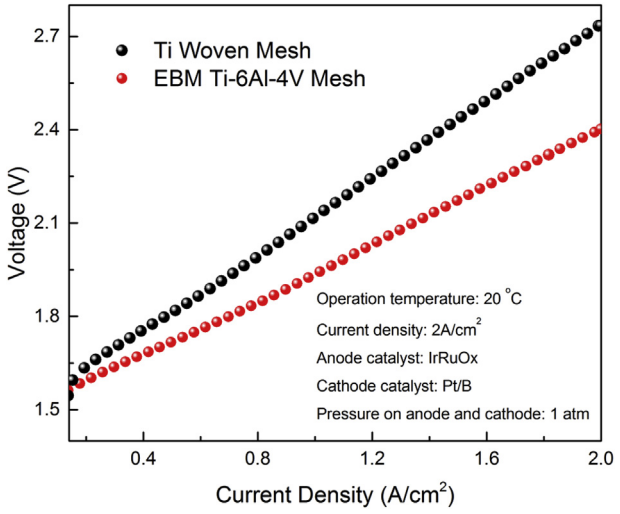

Fig. 6 – Performance curves of PEMEC with anode LGDL of EBM Ti-6Al-4V mesh and Ti woven mesh at room temperature.

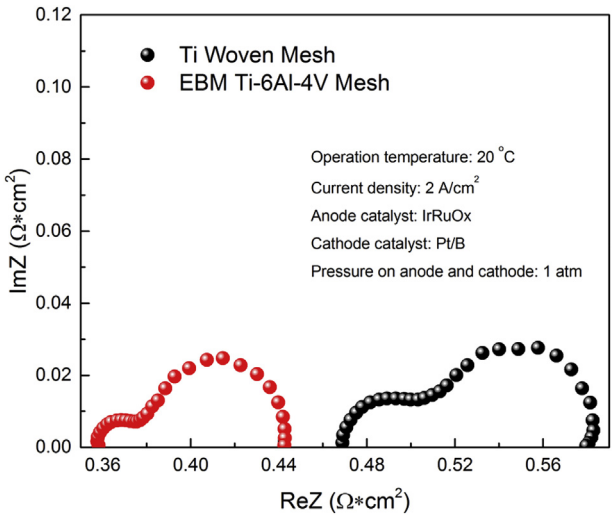

Fig. 7 – GEIS curves of PEMEC with anode LGDL of EBM Ti-6Al-4V LGDLs and Ti woven mesh under the current density of 2 A/cm^2 at room temperature.

For a better understanding of the performance data, GEIS testing was conducted *in-situ* with both titanium woven and EBM Ti-6Al-4V LGDLs. Fig. 7 shows the Nyquist plots of the impedances with EBM Ti-6Al-4V LGDLs and Ti woven LGDLs under the current density of 2 A/cm^2 at room temperature. The scanning frequency was from 10 kHz to 5 mHz, and recorded six points of data per decade. The ohmic loss, which was derived from their leftmost x-intercepts at a high frequency range, was significantly decreased from 0.47 Ω cm^2 to 0.36 Ω cm^2 with woven mesh and EBM Ti-6Al-4V LGDLs respectively. This phenomenon can be explained by the distinct structures and morphologies between two meshes. With the flat and in-plane surface, the EBM Ti-6Al-4V printing LGDL provides a better contact with both current distributors and catalyst coated membranes (CCMs), as shown in Figs. 3 and 4, which significantly decrease the contact resistance, thus making the ohmic loss less than woven meshes.

The PEMEC performance was further enhanced at higher operating temperatures, as shown in Fig. 8. The cell temperature is varied from 35 to 65 °C at a step of 15 °C, which is within the general operating temperature region in the PEMEC system [13]. At 1.5 A/cm^2, the operating voltage needed was 2.13 V, 2.02 V and 1.91 V, respectively, which indicated a significant performance improvement. Higher temperature in PEMECs promotes improved kinetics and interfacial contacts, enhances the proton conductivity inside the membrane, and enhances the diffusion of reactants while decreasing the concentration difference [12,20,32].

As shown in Fig. 9, the GEIS results indicated that the ohmic loss reduced remarkably along with the increasing of cell temperature. At 35 °C, its ohmic loss was about 0.33 Ω cm^2, while at higher temperature of 65 °C, it was reduced to 0.21 Ω cm^2, which lead to a lower voltage (better performance). The major impact on the ohmic loss is the change of

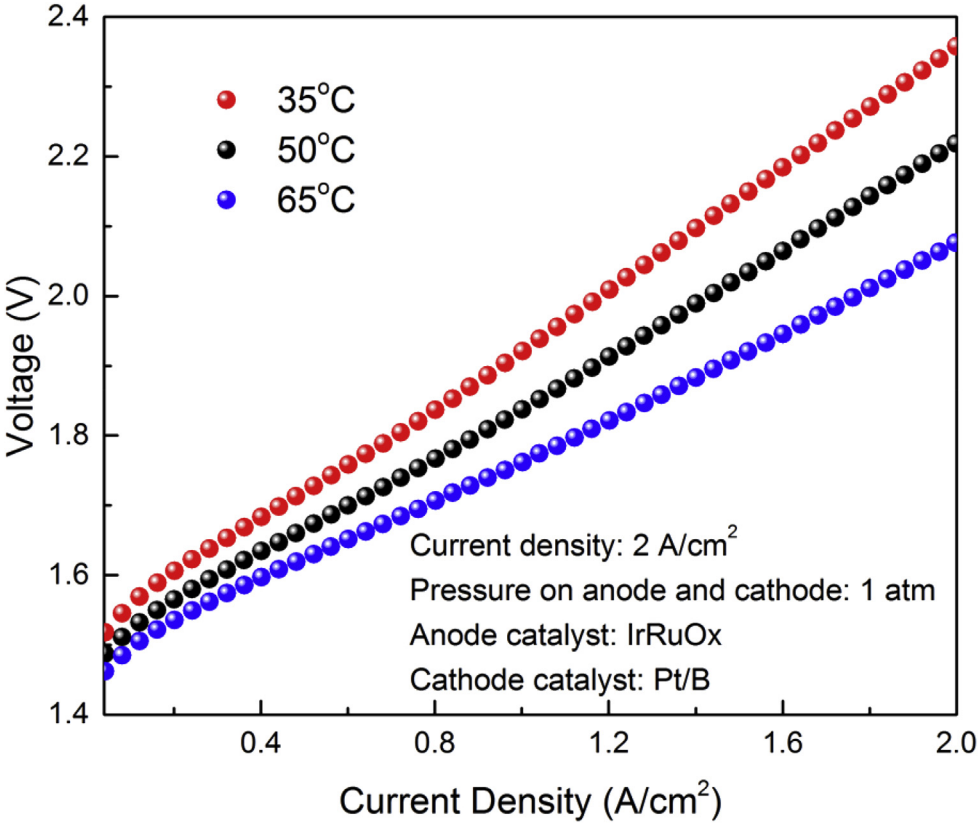

Fig. 8 – Performance results of PEMEC with anode LGDL of EBM Ti-6Al-4V mesh at different temperatures.

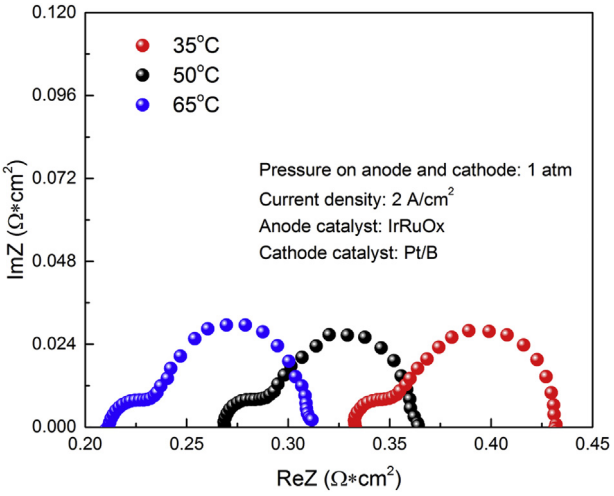

Fig. 9 – GEIS results of PEMEC with anode LGDL of EBM Ti-6Al-4V mesh at different temperatures.

interfacial contact resistance along with the increasing of operation temperature. The higher operation temperature will expand the components inside the PEMEC, tighten the components and then reduce the interfacial contact resistance, which can't be achieved by increasing the torque of fasten bolts as aforementioned.

It has been shown that ohmic losses play a dominant role in PEMEC performance, and its reduction will directly result in lowering the operating voltage of the PEMEC, thus promoting performance and efficiency. With EBM Ti-6Al-4V technology, LGDLs with different pore morphologies and structures, including pore size, shape, wall thickness, and porosity can be easily manufactured for further reducing the ohmic resistance and enhancing performance in a PEMEC.

Conclusion

A low-cost technique of the electron beam melting (EBM) additive manufacturing for fabricating titanium liquid/gas diffusion media with high-corrosion resistance and well-tunable multifunctional parameters has been demonstrated for the first time. Their applications in proton exchange membrane electrolyzer cells have been explored. By taking advantage of the additive manufacturing, the EBM technology makes it possible to fabricate a three-dimensional and complicated object of virtually any shape from a digital model faster, cheaper, and easier than conventional methods, especially for titanium. In addition, compared with conventional woven LGDLs, increased performance and efficiency of up to 8% at room temperature with EBM Ti-6Al-4V LGDLs is obtained due to their significant reduction of ohmic losses. More importantly, this process can enable manufacturing of LGDLs with control of pore size, pore shape, pore distribution, and therefore porosity and permeability, which will be valuable in developing sophisticated PEMEC models, which will in turn allow the optimization of the LGDL for maximum performance. Further, it will lead to a manufacturing solution to couple the LGDLs with other parts, since they can be easily integrated together with this advanced manufacturing process. Further optimal investigations and improvements of the EBM Ti-6Al-4V LGDLs and other components are underway.

Acknowledgments

The authors greatly appreciate the support from U.S. Department of Energy's National Energy Technology Laboratory under Award DE-FE0011585, and Office of Energy Efficiency and Renewable Energy, Advanced Manufacturing Office, under contract DE-AC05-00OR22725 with UT-Battelle, LLC. The authors also wish to express their appreciation to Stuart Steen, Dr. Bo Han, Zhengye, Kang, William Barnhill, Douglas Warnberg, and Rong Chen for their help.

REFERENCES

[1] Vanhanen JP, Lund PD, Tolonen JS. Electrolyser – metal hydride – fuel cell system for seasonal energy storage. Hydrogen Energy Prog Xi 1996;1–3:995–1004.
[2] Turner J, Sverdrup G, Mann MK, Maness PC, Kroposki B, Ghirardi M, et al. Renewable hydrogen production. Int J Energy Res 2008;32(5):379–407.
[3] Ayers KE, Anderson EB, Capuano C, Carter B, Dalton L, Hanlon G, et al. Research advances towards low cost, high efficiency PEM electrolysis. ECS Trans 2010;33(1):3–15.
[4] Debe MK, Hendricks SM, Vernstrom GD, Meyers M, Brostrom M, Stephens M, et al. Initial performance and durability of ultra-low loaded NSTF electrodes for PEM electrolyzers. J Electrochem Soc 2012;159(6):K165–76.
[5] Toops TJ, Brady MP, Zhang F-Y, Meyer HM, Ayers K, Roemer A, et al. Evaluation of nitrided titanium separator plates for proton exchange membrane electrolyzer cells. J Power Sources 2014;2014(272):954–60.
[6] Yang H, Guo L, Yan W, Liu H. A novel composite photocatalyst for water splitting hydrogen production. J Power Sources 2006;159(2):1305–9.
[7] Hatzell KB, Beidaghi M, Campos JW, Dennison CR, Kumbur EC, Gogotsi Y. A high performance pseudocapacitive suspension electrode for the electrochemical flow capacitor. Electrochim Acta 2013;111:888–97.
[8] Zoulias E, Varkaraki E, Lymberopoulos N, Christodoulou CN, Karagiorgis GN. A review on water electrolysis. TCJST 2004;4(2):41–71.
[9] Chisholm G, Kitson PJ, Kirkaldy ND, Bloor LG, Cronin L. 3D printed flow plates for the electrolysis of water: an economic and adaptable approach to device manufacture. Energy Environ Sci 2014;7(9):3026–32.
[10] Song SD, Zhang HM, Ma XP, Shao ZG, Baker RT, Yi BL. Electrochemical investigation of electrocatalysts for the oxygen evolution reaction in PEM water electrolyzers. Int J Hydrogen Energy 2008;33(19):4955–61.
[11] Carmo M, Fritz DL, Merge J, Stolten D. A comprehensive review on PEM water electrolysis. Int J Hydrogen Energy 2013;38(12):4901–34.
[12] Han B, Steen SM, Mo J, Zhang F-Y. Electrochemical performance modeling of a proton exchange membrane electrolyzer cell for hydrogen energy. Int J Hydrogen Energy 2015;40(22):7006–16.

[13] Ma LR, Sui S, Zhai YC. Investigations on high performance proton exchange membrane water electrolyzer. Int J Hydrogen Energy 2009;34(2):678–84.
[14] Zenyuk I, Kumbur E, Litster S. Deterministic contact mechanics model applied to electrode interfaces in polymer electrolyte fuel cells and interfacial water accumulation. J Power Sources 2013;241:379–87.
[15] Swamy T, Kumbur E, Mench M. Characterization of interfacial structure in PEFCs: water storage and contact resistance model. J Electrochem Soc 2010;157(1):B77–85.
[16] Kalidindi A, Taspinar R, Litster S, Kumbur E. A two-phase model for studying the role of microporous layer and catalyst layer interface on polymer electrolyte fuel cell performance. Int J Hydrogen Energy 2013;38(22):9297–309.
[17] Mo J, Steen III SM, Han B, Zhang F-Y. High-speed and micro-scale measurements of flow and reaction dynamics for sustainable energy storage. In: 13th International Energy Conversion Engineering Conference; 2015.
[18] Higier A, Liu H. Optimization of PEM fuel cell flow field via local current density measurement. Int J Hydrogen Energy 2010;35(5):2144–50.
[19] Kumbur E, Sharp K, Mench M. On the effectiveness of Leverett approach for describing the water transport in fuel cell diffusion media. J Power Sources 2007;168(2):356–68.
[20] Owejan JP, Trabold TA, Mench MM. Oxygen transport resistance correlated to liquid water saturation in the gas diffusion layer of PEM fuel cells. Int J Heat Mass Transf 2014;71:585–92.
[21] Mo J, Steen SM, Zhang F-Y, Toops TJ, Brady MP, Green JB. Electrochemical investigation of stainless steel corrosion in a proton exchange membrane electrolyzer cell. Int J Hydrogen Energy 2015;40(36):12506–11.
[22] Zhang F-Y, Advani SG, Prasad AK. Performance of a metallic gas diffusion layer for PEM fuel cells. J Power Sources 2008;176(1):293–8.
[23] Arisetty S, Prasad AK, Advani SG. Metal foams as flow field and gas diffusion layer in direct methanol fuel cells. J Power Sources 2007;165(1):49–57.
[24] Wang H, Turner JA. Reviewing metallic PEMFC bipolar plates. Fuel Cells 2010;10(4):510–9.
[25] Zhang F-Y, Prasad AK, Advani SG. Investigation of a copper etching technique to fabricate metallic gas diffusion media. J Micromech Microeng 2006;16(11):N23.
[26] Mo J, Steen SM, Retterer S, Cullen DA, Terekhov A, Zhang F-Y. Mask-patterned wet etching of thin titanium liquid/gas diffusion layers for a PEMEC. ECS Trans 2015;66(24):3–10.
[27] Manahan M, Hatzell M, Kumbur E, Mench M. Laser perforated fuel cell diffusion media. Part I: related changes in performance and water content. J Power Sources 2011;196(13):5573–82.
[28] Joshi PC, Dehoff RR, Duty CE, Peter WH, Ott RD, Love LJ, et al. Direct digital additive manufacturing technologies: path towards hybrid integration. In: Future of Instrumentation International Workshop (FIIW), 2012. IEEE; 2012.
[29] Sames WJ, Unocic KA, Dehoff RR, Lolla T, Babu SS. Thermal effects on microstructural heterogeneity of Inconel 718 materials fabricated by electron beam melting. J Mater Res 2014;29(17):1920–30.
[30] Dinwiddie RB, Dehoff RR, Lloyd PD, Lowe LE, Ulrich JB. Thermographic in-situ process monitoring of the electron-beam melting technology used in additive manufacturing. In: SPIE Defense, Security, and Sensing. International Society for Optics and Photonics; 2013.
[31] Zheng HY, Ito H, Okabe TH. Production of titanium powder by the calciothermic reduction of titanium concentrates or ore using the preform reduction process. Mater Trans 2007;48(8):2244–51.
[32] Zhou T, Liu H. Effects of the electrical resistances of the GDL in a PEM fuel cell. J Power Sources 2006;161(1):444–53.